

Quantum Theory of Čerenkov Radiation, Spectral Cutoff and Resonances

Ido Kaminer¹, Maor Mutzafi², Gal Harari², Hanan Herzig Sheinfux²,
Amir Levy¹, Scott Skirlo¹, Jonathan Nemirovsky², John D. Joannopoulos¹,
Mordechai Segev², and Marin Soljačić¹

¹Department of Physics, Massachusetts Institute of Technology, 77 Massachusetts Avenue,
Cambridge, Massachusetts, USA

²Physics Department and Solid State Institute, Technion, Haifa 32000, Israel

[email: kaminer@mit.edu](mailto:kaminer@mit.edu)

Abstract:

We show that the well-established Čerenkov Effect contains new phenomena arising directly from the quantum nature of the charged particles. These include large deviations from the classically-expected radiation intensity and angle. Most importantly, we find that the traditional Čerenkov angle splits, confining the emitted radiation into two distinctive cones into which two photonic shock waves are emitted. Interestingly, one of the two shockwaves can move on a backward cone, which is otherwise considered impossible for Čerenkov Radiation in ordinary materials. Moreover, for specific values of the particle momentum, we predict an upper frequency cutoff in the photon emission. Surprisingly, for this extremum frequency we find a diverging rate of photon emission, implying this is a new resonant light-matter interaction. Some of these new effects cannot be found without the full quantum derivation. Importantly, our findings are observable for electron beams with realistic parameters, offering new applications including coherent x-ray sources and open a new realm for Čerenkov detectors.

Introduction

When a charged particle travels faster than the phase velocity of light in a medium, it produces Čerenkov radiation (ČR). Although it is now 80 years since its first observation by Čerenkov [1], surprisingly little attention was given to the importance of the quantum nature of the charged particles producing the radiation. Since its discovery, the Čerenkov Effect has become a fundamental part of many fields [2]: It is responsible for the bluish glow of nuclear reactors, and is being used to characterize radioactivity of fuel rods [3]; Devices like the Ring-imaging Čerenkov detector are used for particle identification in high-energy physics experiments [4-8], and for cosmic radiation measurements in astrophysics [9,10]; It is serving as the basis of novel acceleration methods [11], and even as an unusual imaging tool in biology [12,13]. The fundamental nature of ČR has led to an incredible amount of research that continues to this day, as novel Čerenkov-related effects are being found in previously unexplored settings and even in modern nanostructures, including photonic crystals [14] and metamaterials [15]. Importantly, despite the immense progress, researchers still regard the effect as the electromagnetic field emitted by a **point charge** moving with a relativistic speed, or a collection thereof. This is the exact same theory (henceforth referred to as the conventional theory) developed in 1937 by Frank and Tam [16], who later shared the Nobel Prize in Physics of 1958 with Čerenkov, for explaining his observation.

In fact, those few studies that did address the Čerenkov Effect in a quantum mechanical formalism, have found excellent correspondence to the conventional theory. Namely, in 1948 [17] ČR was re-derived by considering an electron as a single momentum state (a plane-wave) interacting with a photon through the Dirac Hamiltonian. That work has shown that the only

correction to the Frank-Tamm formula occurs for extremely energetic photons, with energy close to the rest mass of the electron. Other early works considered a Hamiltonian that also quantized the medium, in order to study the implications of materials' resonances, as a correction to the homogenized permittivity in the conventional ČR (e.g. [18]). A 1957 paper [19] showed how the possibility of two-photon emission affects the ČR, with later works providing experimental observation of such corrections arising from higher order Feynman diagrams [20]. A quantum mechanical formalism was also used to describe the radiation emitted by an electron passing through a medium in the presence of an external magnetic field, giving rise to the synergic synchrotron-Čerenkov radiation [21,22]. There, the derivation of the quantum correction [21] shows a phase-transition near the ČR threshold, where critical fluctuations arise directly from the quantum terms. More recent works have generalized ČR to more complex physical scenarios, like the nonlinear response of vacuum due to quantum electrodynamics (QED) corrections [23], or hypothetical models such as Lorentz-violating Hamiltonians [24], and faster-than-light particles (tachyons) [25,26]. However, to the best of our knowledge, all previous research always reconfirmed the same classical limit found by Čerenkov, Frank and Tamm [1,16]. In fact, no previous work has ever predicted that the quantum properties of the particle may cause significant deviation from the conventional ČR.

Here, we study the Čerenkov radiation emitted from charged particles described by a quantum wavepacket. For this goal, we develop a matrix elements formalism for scattering of an incoming spin $\frac{1}{2}$ particle into another spin $\frac{1}{2}$ particle and a photon, spanning them by a basis of Bessel-like cylindrical states. Through this formulation, we predict an upper frequency cutoff, above which the ČR is zero. Immediately below this cutoff, we find a resonance in the emission rate, manifested

in a diverging resonant transition rate occurring for particles with velocity close to the critical velocity for ČR. This frequency cutoff and the immediate resonance represent a clear deviation from the conventional ČR theory that displays no such cutoff whatsoever. Moreover, we find complete closed-form expressions for the photon emission rate, showing that the resonance emission is sensitive to the incoming particle spin and the polarization of the emitted photon. This implies that certain spin flip transitions can dominate the process, even when the emitted photon is in the optical range, created from a modestly relativistic electron. Importantly, we show that the effects are not specific for a particular choice of incident wavepackets, but persist for general relativistic cylindrical wavepackets. As such, our predictions should occur in many experimental scenarios, without special engineering of the particle wavepacket. These new effects can have promising applications such as enhanced Čerenkov detectors, creation of new sources of coherent radiation, and new methods for particle acceleration by enhanced Inverse-Čerenkov Effect. These new insights arise from the quantum ČR calculations, and reveal several new phenomena, including photon emission along a backward cone, and a significant deviation from the Čerenkov angle for high energy photons.

The effects of specific wavepackets of the charged particle on ČR is related to many fundamental questions arising from the quantum aspects of the emitted radiation, such as its angular momentum and entanglement. This issue is of great interest today, because it recently became possible to shape the quantum wavepacket of a single electron, imprinting it with orbital angular momentum (OAM) [27-30] or with other intriguing shapes [31].

The conventional theory of the Čerenkov Effect

We begin by recalling the conventional theory of the ČR (Frank-Tamm [16,32]). It consists of a relativistic point charge moving with velocity $v = \beta c$ inside a homogeneous medium with refractive index n , where the speed of light is denoted by c and the normalized electron velocity by β . When the particle velocity is larger than the phase velocity of light in the medium, i.e. $\beta > 1/n$, radiation is emitted and follows a cone with the spread angle $\theta_{ph} = \theta_{\check{C}R}^{conventional}$. The intensity of this emitted radiation can be translated to a dimensionless rate of photon emission per unit frequency Γ_{ω} which is found to be independent of the photon frequency ω . Altogether, the conventional ČR can be summarized in the following two equations:

$$\cos(\theta_{\check{C}R}^{conventional}) = (\beta n)^{-1} \quad (1a)$$

$$\Gamma_{\omega} = \alpha \beta \sin^2(\theta_{\check{C}R}^{conventional}) \quad (1b)$$

with α being the fine structure constant ($\approx 1/137$). Equations 1a,b are a direct outcome of the Maxwell equations with the derived electric and magnetic fields taken to the far-field limit, and a charge/current source being a moving delta function source (point particle). However, in the physical world point particles are never an exact description –all particles in reality have some statistical distributions to their position and momentum or even quantum uncertainty. e.g., their momentum is characterize by some spread angle and some distribution of a finite width. These important characteristics are typically ignored without any significant impact on the results. But as we show in our calculations, they would make an important difference for the ČR.

Several papers have dealt with the ČR in a quantum mechanical context (e.g., [17-19]), but always considered the particle as a single momentum state, analogous to a “plane-wave”

wavepacket in space. Under such an assumption, it was shown that one can re-derive the original equation for the rate Eq.1b. But a “plane-wave” description of a particle, being a single momentum state, is exactly a delta function in momentum space. Such a description is just as problematic as the classical description assuming a delta function in space. Real charge carriers are neither plane waves of a single momentum, nor singular point sources given by delta functions in space. It is this additional feature – of the **coherent superposition of plane waves with different momentum direction** whose interference makes up the quantum wavepacket of an electron – that gives rise to major deviations from the conventional theory of ČR, and the new effects we predict here. Consequently, by engineering the quantum wavepacket we can greatly enhance the predicted effects and show additional effects that are unique to specially shaped quantum particles. A direct implication is that one can control the ČR by shaping an incoming electron beam to a certain structure to its wavepacket. Note that from now on, we call our particle “electron”, even though the results are exactly the same for any spin-1/2 fermion (since we have no assumptions in respect to the mass). Moreover, the generalization for particles with any spin is straightforward, only changing the spinor-dependent terms (only the last two equations here).

Introducing the formalism: the quantum approach to the Čerenkov Effect

In QED the meaning of a wavepacket is that the initial state is a sum (or integral) over creation operators of single electrons, where each usually describes an electron of a single momentum state. We choose to describe these single electron states in momentum space using cylindrical coordinates, so that every state is defined by $|p_i^{cyl}\rangle = |E_i, s_i, \theta_i, l_i\rangle$, which contains its energy E_i , spin s_i , spread angle θ_i , and OAM l_i respective to the cylinder axis (z). An equivalent notation, which we use in some cases below, has the longitudinal and transverse momenta, related to θ_i by

$p_{iz} = \beta E_i \cos(\theta_i) / c$ and $p_{ir} = \beta E_i \sin(\theta_i) / c$ respectively ($\beta = \beta_i$ is the regular normalized speed, related to the energy by $E_i = (1 - \beta^2)^{-1/2} mc^2$). See Fig.1 for an illustration of the states and the notations. When presenting this state in real-space – it has a Bessel function-like profile – as recently shown in [33] as wavepacket solutions of the Dirac equation.

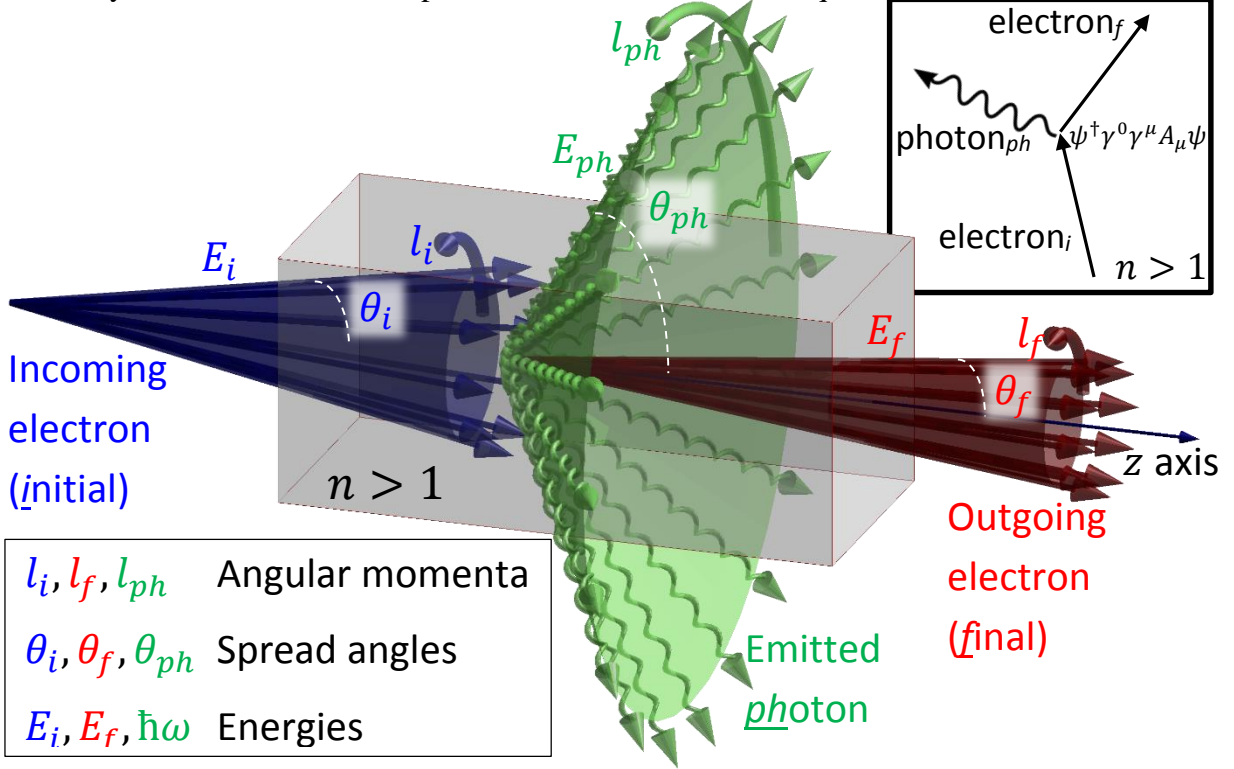


Figure 1: A schematic illustration of the ČR process we calculate. The incoming (outgoing) electron is plotted in blue (red), with its state described by a longitudinal momentum $p_{iz} = p_i \cos(\theta_i)$ ($p_{fz} = p_f \cos(\theta_f)$), a transverse momentum $p_{ir} = p_i \sin(\theta_i)$ ($p_{fr} = p_f \sin(\theta_f)$), and an angular momentum l_i (l_f). The emitted photon is plotted in green, with its state described by a longitudinal wavenumber $k_z = n\omega \cos(\theta_{ph})/c$, a transverse wavenumber $k_r = n\omega \sin(\theta_{ph})/c$ and an angular momentum l_{ph} .

To describe the ČR in QED, we consider the spin-polarization term in the Dirac Hamiltonian $\psi^\dagger \gamma^0 \gamma^\mu A_\mu \psi$, describing the electron-photon interaction. Where ψ (ψ^\dagger) are the electron annihilation (creation) operator, and A_μ is the photon annihilation operator. We impose the simplest final state, of a single electron and a single photon, both described in cylindrical coordinates by $|p_f^{cyl}\rangle \otimes |k^{cyl}\rangle = |E_f, s_f, \theta_f, l_f\rangle \otimes |\hbar\omega, s_{ph}, \theta_{ph}, l_{ph}\rangle$ (see Fig.1). The electron parameters are as above, while the photon is characterize by its frequency ω , spin s_{ph} (which is

the azimuthal/radial polarization), emission angle θ_{ph} , and OAM l_{ph} . In some cases below we also use the longitudinal and transverse photon wavenumbers, related to θ_{ph} by $k_z = n\omega \cos(\theta_{ph})/c$ and $k_r = n\omega \sin(\theta_{ph})/c$ respectively (the dispersion relation of the photon is $\omega = |\vec{k}|nc$). In a medium where $n > 1$, this final state is created by a first-order interaction from an initial state of a single electron, and is ***the only possible first-order interaction***, hence it is the dominant effect. This first-order interaction does not occur in vacuum, because conservation of energy and momentum cannot be satisfied together.

The quantum derivation. First step: the bra-ket expression

The first step in describing the transition shown in Fig.1 ($p_i^{cyl} \rightarrow p_f^{cyl} + k^{cyl}$) is writing the bra-ket expression:

$$\begin{aligned}
M_{p_i^{cyl} \rightarrow p_f^{cyl} + k^{cyl}}^{density}(t, r, \varphi, z) &= \langle p_f^{cyl} \text{ electron}, k^{cyl} \text{ photon} | \underbrace{\psi^\dagger \gamma^0 \gamma^\mu \psi}_{\hat{=} j^\mu(t, r, \varphi, z)} q A_\mu(t, r, \varphi, z) | p_i^{cyl} \text{ electron}, 0 \rangle \\
&= \underbrace{\left[\frac{q}{n\sqrt{\varepsilon_0}} \frac{\hbar c}{\sqrt{\hbar\omega}} \frac{1}{\sqrt{\pi L_r^2 L_z}} \right]}_{q A_\mu \text{ normalization}} \underbrace{\frac{1}{\pi L_r^2 L_z}}_{j^\mu \text{ normalization}} \exp\left(i \frac{1}{\hbar} (p_{iz} - p_{fz}) z - i k_z z\right) \exp\left(i\omega t - i \frac{1}{\hbar} (E_i - E_f) t\right) \quad (2) \\
&\cdot \left[e^{il_f\varphi} J_{l_i} \left(\frac{1}{\hbar} p_{ir} r \right) \right] \left[e^{-il_f\varphi} J_{l_f} \left(\frac{1}{\hbar} p_{fr} r \right) \right] \left[e^{-i(l_{ph}+1)\varphi} J_{l_{ph}+1}(k_r r) \right] \underbrace{\left[\frac{p_{fz}(E_i + mc^2) - p_{iz}(E_f + mc^2)}{\sqrt{E_i} \sqrt{E_f} \sqrt{E_i + mc^2} \sqrt{E_f + mc^2}} \right]}_{\text{spinor-polarization term}}
\end{aligned}$$

Where the normalization of the current operator $j^\mu \hat{=} \psi^\dagger \gamma^0 \gamma^\mu \psi$ uses the volume of the cylindrical space of radius L_r and length L_z which will be taken to infinity later. In the normalization of the photon field operator A^μ , ε_0 is the vacuum permittivity. The radial dependence is given in the form of Bessel functions, due to the cylindrical symmetry. We use the term $M^{density}(t, r, \varphi, z)$ to stress that the actual matrix element still requires integrating over space-time, since Eq.2 is based on the

Hamiltonian density. Notice that Eq.2 is given for the special case of the electron flipping its spin and the photon having an azimuthal polarization. Each spin and choice of polarization results in a different spinor-polarization term, and in a change in the orders of the Bessel functions. The full description of all cases is given in [34].

A simpler version of this calculation was described in [17,18,35,36], where both electrons and photons are described by a single momentum state, i.e., plane waves. One might wonder why not take a superposition of such simple states and construct any general wavepacket this way. These works [17,18,35,36] even show that Eq.1b is reached from the QED derivation when the particle is this single momentum state. Would a mere superposition of the emission rate in Eq.1b be already enough to describe the ČR of an incoming electron wavepacket? The answer is no. It is of course possible to compose any wavepacket from a plane wave basis, yet there is no linear relation guaranteeing that the resulting ČR could be given as a simple superposition. In fact – it is exactly the opposite: the process of radiation creation is nonlinear, hence there are cross-terms that have to be taken into account when calculating the total emitted radiation. These cross-terms mean that the radiation from different parts of the incoming wavepacket (e.g., from different plane wave constituents) have to be added up coherently, when combined together in the calculation of the emitted photon at each angle specifically. Due to these cross-terms, the “plane-wave” basis is not a good choice here. Instead, we find it more convenient to use a cylindrical basis when spanning more complicated (and more realistic) wavepackets, such as Gaussian wavepackets, or basically any “beam” as long as it is cylindrically symmetric. This basis gives us a very strong mathematical framework since all cross-terms can vanish when the wavepacket has cylindrical symmetry – therefore it is the most natural for this kind of problems.

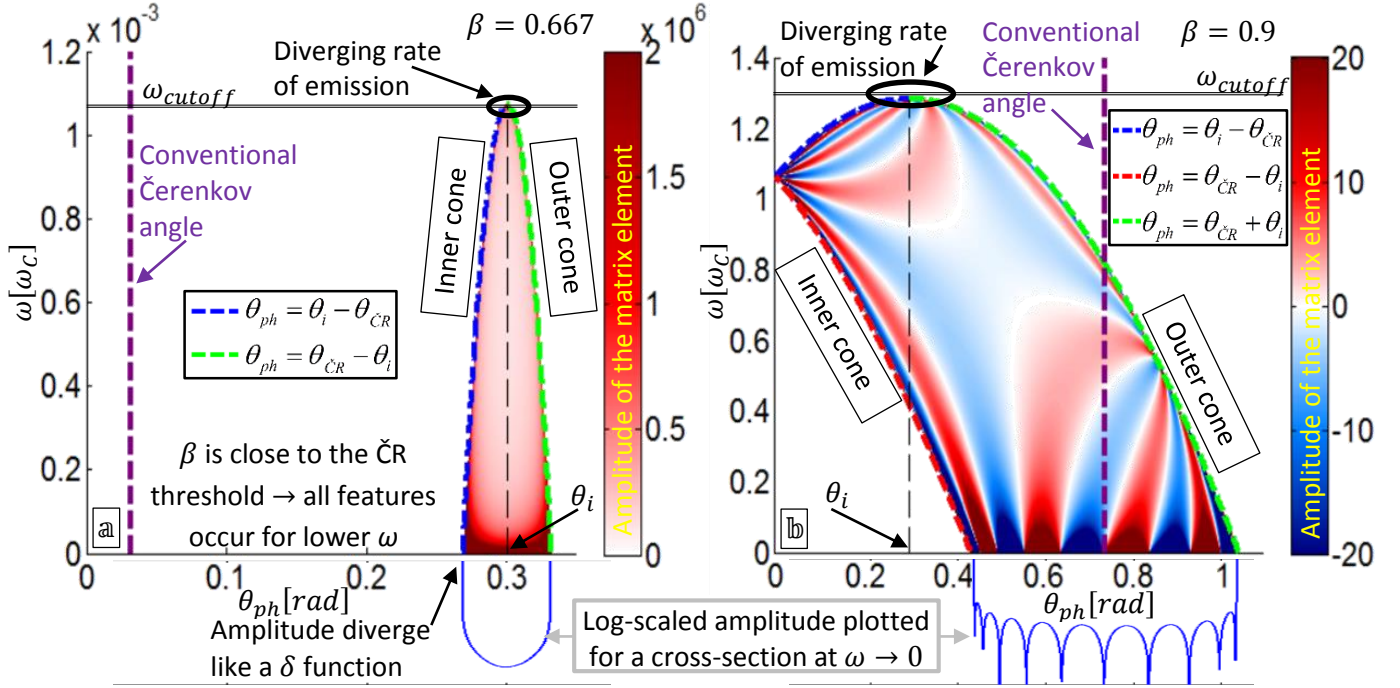
The quantum derivation. Second step: the matrix element

The second step in describing the transition $p_i^{cyl} \rightarrow p_f^{cyl} + k^{cyl}$ requires integrating Eq.2 over space-time, giving the matrix element (or the transition amplitude). We get δ functions for the conservation of energy, longitudinal momentum, and angular momentum. The remaining integral over the cylindrical radius r involves the three Bessel functions, which was fortunately studied in the mathematical literature [37] providing us with an analytic:

$$\int_0^{\infty} J_{l_i}(p_{ir}r/\hbar) J_{l_f}(p_{fr}r/\hbar) J_{l_{ph}+1=l_i-l_f}(k_r r) r dr = \frac{\cos(l_i\alpha_f - l_f\alpha_i)}{2\pi S_{\Delta}(\frac{1}{\hbar} p_{ir}, \frac{1}{\hbar} p_{fr}, k_r)} \quad (3)$$

Where S_{Δ} is the area of a triangle formed by sides with the lengths $\frac{1}{\hbar}p_{ir} = \frac{1}{\hbar}p_i \sin(\theta_i)$, $\frac{1}{\hbar}p_{fr} = \frac{1}{\hbar}p_f \sin(\theta_f)$, and $k_r = n\omega \sin(\theta_{ph})/c$, where α_i , α_f , and α_{ph} are the angles opposite the three sides respectively. If a triangle cannot be made, then the integral is zero, which gives another selection rule (though not a simple one) for the possible radiation emission. When combined with the conservation of energy momentum and angular momentum, this selection rule defines a finite regime shown in Figs.2a,b. Most importantly, the amplitude always diverges on the edge of the regime (blue/red/green dashed lines in Figs.2a,b), since this is where the triangle area S_{Δ} goes to zero. The integral of Eq.3 also appeared in a study of scalar Compton backscattering [38,39], where a similar mathematical framework is used to describe charged particles carrying OAM, interacting with incoming photons also carrying OAM. There, the authors also discussed the case of finite transverse dimension limiting the integral [39], the nature of the S_{Δ}^{-1} divergence (appendixes of [38]), and the selection rules mentioned above, although in the spinless case [38]. This shows that our calculations can describe additional physical phenomena such as the Compton Effect from electrons or other fermions (since we solve the full vector case – i.e., taking into account the spin).

In section II of [34] we show another result related to the integral of Eq.3, expressing it as a sum of delta functions, in the sense of a distribution [40].



The matrix elements amplitudes for the Čerenkov emission process, plotted as a function of the photon frequency ω and spread angle θ_{ph} , for two values of the incoming charge velocity: $\beta = 0.667$ (left panel) and $\beta = 0.9$ (right panel). Distinct features (“stripes”) are found for different OAM carried by the emitted photon (the current figures are plotted for $l_{ph}=10$). The amplitudes here show the spatial part of the matrix element (Eq.3), which vanishes outside of the permitted zone, marked by the blue, red and green dashed curves. Along these curves the amplitude contains a delta-like divergence thus we use a saturated color scale, with darker color corresponding to higher transition amplitudes. These divergences are emphasized by the cross-section plots below the maps. The purple dashed curve denotes the angle of the conventional ČR (Eq.1a), which equals 0.0316 for the left panel and 0.7366 for the right panel. The upper cutoff frequency is marked by a doubled black line – above it no photons are emitted (see Eq.4). This is in direct contrast to the conventional theory of ČR, for which there is no upper frequency cutoff. Along the cutoff line we mark the divergence of the emission rate by black ellipses, exactly where the curve slope goes to zero, consistent with the photonic density of states going to infinity. All figures are plotted for $n = 1.5$ and $\theta_i = 0.3$, with a spin-flip transition emitting an azimuthally polarized photon, yet the features exist for any choice of parameters. ω is in units of the Compton frequency $\omega_c = mc^2/\hbar$.

Due to the divergence along the edges, the photon emission only occurs along discrete angles $\theta_{ph} = |\theta_i \pm \theta_{\check{C}R}|$ marked by the blue/red/green dashed lines. The notation $\theta_{\check{C}R}$ can be found analytically, and can also be derived from elementary conservation laws:

$$\theta_{\check{C}R} = \arccos\left(\frac{1}{\beta n} + \frac{\omega}{\omega_c} \frac{\sqrt{1-\beta^2}}{\beta} \frac{n^2-1}{2n}\right), \quad (4)$$

where $\omega_c = mc^2/\hbar$ is the Compton frequency, given by the rest energy of the electron divided by the reduced Planck Constant. For the limit case of $\theta_i = 0$, our incoming electron state $|p_i^{cyl}\rangle$

reduces to a plane wave (single momentum state), and then the radiation spread angle is just $\theta_{ph} = \theta_{\check{C}R}$ (purple dashed line), generalizing Eq.1a. This special case matches different derivations in the literature, done first in 1944 [41], and later under different approximations and assumptions [17,18,35,36]. Our general case of an incoming $|p_i^{cyl}\rangle$, uses $\theta_{\check{C}R}$ as a convenient mathematical notation, and does not represent the angle of photon emission θ_{ph} – see the difference of the purple vs. the blue/red/green dashed lines. This significant difference has an important physics implication: the $|p_i^{cyl}\rangle$ electron has **two** allowed angles of ČR emission for each ω , resulting in a double Čerenkov cone, which we name the inner-cone and outer-cone.

The most important physical consequence emphasized in Figs.2a,b is marked by the double black line that bounds the range of emission. This is in contradiction to Eqs.1a,b that have no bound and are even frequency independent – the conventional ČR is famously broad in spectrum, truncated only by the material dispersion (when $n = n(\omega)$ drops towards 1 and gets below $1/\beta$). Nevertheless, the quantum derivation yields a fundamental frequency cutoff that does not depend on the material dispersion:

$$\omega_{cutoff} = 2\omega_c \frac{\beta n - 1}{(n^2 - 1)\sqrt{1 - \beta^2}}, \quad (5)$$

The fact that a frequency cutoff does exist for some extreme parameters is expected– a trivial reason being that a charged particle cannot create a photon carrying more energy than it originally had. However, a particularly interesting implication of this formula, which as far as we know was not noted before, concerns low frequency photons (e.g., Fig.1a): Near the Čerenkov threshold the velocity satisfies $\beta \approx 1/n$, and thus ω_{cutoff} shifts to very low frequencies. Equation 5 shows that the cutoff is linear in $\beta - 1/n$, with a very large slope ($\sim mc^2/\hbar$). In theory, taking a charged particle with a velocity arbitrarily close to the Čerenkov threshold would shift the frequency cutoff

all the way to zero. In practice, this is only possible up to the experimental precision one can have in setting the velocity of the charged particle, or equivalently, its energy variance. Fortunately, variances in the electron energy in modern electron guns is already low enough. For example, transmission electron microscopes (average energy 100-200KeV) can work with a variance in the electron energy that is lower than 1eV, which brings the cutoff to the optical frequencies (2eV photon = wavelength of 620nm, hence 1eV is near-IR). Even when having a larger variance in the electron energy, some signature of the predicted effect can still be observed. This is due to the simple fact that ČR is no longer frequency-independent, as the conventional theory implies. Notice that a related effect was noted in 1976 [21] in the synchrotron-Čerenkov radiation created by an electron wiggled by an external magnetic field, while it moves in a medium with some refractive index n . It reveals a critical point when the electron velocity is near the Čerenkov threshold $\beta \approx 1/n$, causing the magnetic-field-dependent quantum correction term to be amplified, effectively leading to enhanced synchrotron radiation (as the radiation is proportional to the magnetic field $^{(2/3)}$). See [21] section 4(iii)).

Of particular physical importance is the exact point where the colored regimes of Figs.2a,b touch the cutoff frequency line (black ellipse), since there the dashed curve has a zero slope, which implies a diverging photon density of states. This will later lead to certain scenarios of diverging rate of emission. Such a divergence is a clear deviation from the conventional theory, which also persists in arbitrary wavepackets, since our predicted cutoff is independent of the incoming particle spread angle θ_i .

Figure 2b exhibits another intriguing phenomenon of the quantum ČR: there is a single point where the regime touches the ω axis. This point shows that contrary to the conventional ČR theory, there exist emitted photons that go exactly on axis, and these photons are fully coherent, having only a single allowed frequency. This special frequency can be found by substituting $\theta_i = \theta_{\check{C}R}$ in Eq.4 and extracting the frequency, yielding:

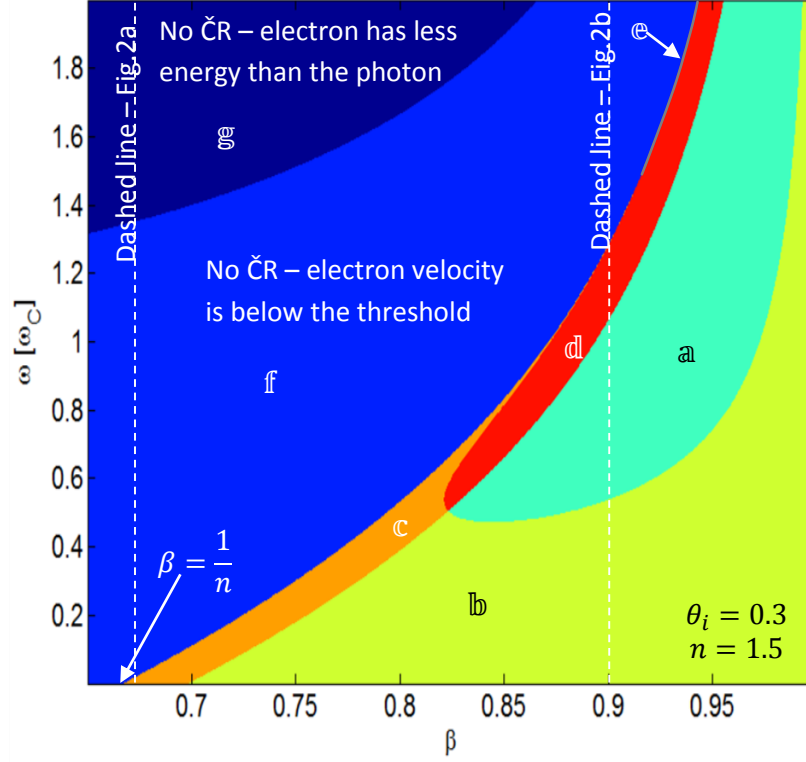
$$\omega_{at \theta_{ph}=0} = 2\omega_C \frac{\beta n \cos(\theta_i) - 1}{(n^2 - 1)\sqrt{1 - \beta^2}} \quad (6)$$

For β close to 1, this frequency corresponds to a gamma-ray photon with energy on the scale of the electron energy. However, this effect can be brought down to much lower frequencies, even in the optical range, by taking the electron velocity close to the Čerenkov threshold ($\beta \approx 1/n$), in much the same way as in Eq.5.

The quantum derivation. Third step: the rate of emission

So far we found the amplitude of a single $p_i^{cyl} \rightarrow p_f^{cyl} + k^{cyl}$ transition. The ČR theory involves all possible transitions at once, thus we sum (integrate) over all emitted electron and photon states. This eliminates the δ functions found in the matrix elements and balance the volume normalization seen in Eqs.2 so when the cylinder volume is taken to infinity we get a result that is independent of the cylinder size. The elaborate calculations needed here to solve the integrals can all be done analytically, eventually giving a surprisingly simple result for the total photon emission Γ_ω (see Eq.7 below). It is comprised of two emission cones, inner ($\theta_{ph} = |\theta_i - \theta_{\check{C}R}|$) and outer ($\theta_{ph} = \theta_i + \theta_{\check{C}R}$), as shown in Figs.2a,b. Each cone has one of three alternative formulas describing its rate of emission Γ_ω that we denote by ČR of type I,II,III and correspond to the three possible ways of satisfying the conservation of transverse momentum. In order to find which ČR

type describe the emission rate at each cone, we calculate the transverse momenta $p_{tr} = \beta E_i \sin(\theta_i)$ and $\hbar k_r = n\hbar\omega \sin(\theta_{ph})$, use the map and table of Fig.3, and the inequalities of Eq.7.



Domain	Inner photon cone		Outer photon cone		Condition
	Spread angle θ_{ph}	Type	Spread angle θ_{ph}	Type	
a	$\theta_{\check{C}R} - \theta_i$	I	$\theta_i + \theta_{\check{C}R}$	II	$\theta_i < \theta_{\check{C}R}$
b	$\theta_{\check{C}R} - \theta_i$	I	$\theta_i + \theta_{\check{C}R}$	III	$\theta_i < \theta_{\check{C}R}$
c	$\theta_i - \theta_{\check{C}R}$	III	$\theta_i + \theta_{\check{C}R}$	III	$\theta_i > \theta_{\check{C}R}$
d	$\theta_i - \theta_{\check{C}R}$	III	$\theta_i + \theta_{\check{C}R}$	II	$\theta_i > \theta_{\check{C}R}$
e	$\theta_i - \theta_{\check{C}R}$	II	$\theta_i + \theta_{\check{C}R}$	II	$\theta_i > \theta_{\check{C}R}$

Map of the 5 domains of ČR vs. the incoming charge velocity β and the emitted photon frequency ω . The blue domains (f&g) allow no ČR because the particle velocity β is not high enough for current $n = 1.5$ (see Eq.5). Domain g is forbidden for any medium since the photon carries more energy than the particle. The domains borders shift as a function of θ_i , and are plotted here for $\theta_i = 0.3$. Note that the border between domain f to the allowed ČR domains is the curve satisfying $\theta_{\check{C}R} = 0$ giving the upper frequency cutoff – on this curve the diverging emission rate can occur for cones of type II and III. Furthermore, two vertical white dashed lines mark the equal-velocity lines for which Figs.2 are plotted. The transitions between different types of ČR that appear in Figs.2 (as the change of dashed line colors) conform to the points where these white dashed lines cross the borders between the domains.

This map highlights the beautiful complexity found by the quantum calculation, where each of its regimes (a-f) corresponds to a unique combination of types for the two ČR cones, as given by the table in Fig.3. It is important to note that in reality, the refractive index varies considerably as a

function of the frequency, hence the entire map should be modified according to the dispersion in the material (alternatively, this map should be read one horizontal line at a time). The total rate of photon emission Γ_ω derived through the quantum framework is eventually:

$$\Gamma_\omega = C \cdot \begin{cases} \frac{\sin(\theta_{ph})}{\sin(\theta_{ph} + \theta_i)} & \frac{1}{\hbar} p_{fr} = k_r + \frac{1}{\hbar} p_{ir} & \text{type I cone} \\ \frac{p_{fr}}{\hbar k_r} \frac{\sin(\theta_{ph})}{\sin(\theta_{ph} - \theta_i)} & k_r = \frac{1}{\hbar} p_{ir} + \frac{1}{\hbar} p_{fr} & \text{type II cone } (p_{ir} < \hbar k_r) \\ \min\left(\frac{p_{fr}}{\hbar k_r}, 1\right) \frac{\sin(\theta_{ph})}{\sin(\theta_{ph} - \theta_i)} & \frac{1}{\hbar} p_{ir} = \frac{1}{\hbar} p_{fr} + k_r & \text{type III cone } (p_{ir} > \hbar k_r) \end{cases} \quad (7)$$

Where the same coefficient C that is shared in all three types of cones differs between different spin-polarization terms and describes in more details in [34] section III. This difference means that the ČR depends on the electron spin, and on the photon polarization, in contrary to the conventional ČR that does not involve any spin whatsoever. Furthermore, this deviation is even enhanced near the cutoff (Eq.5), since Eq.4 gives $\theta_{\check{C}R} \rightarrow 0$ leading to $\theta_{ph} \rightarrow \theta_i$. Then, the denominator of Eq.7 goes zero for cones of types II and III and the total rate Γ_ω *diverges* (except for the case of radial polarization and no spin-flip [34]).

The quantum derivation. Forth step: the spin-polarization contribution

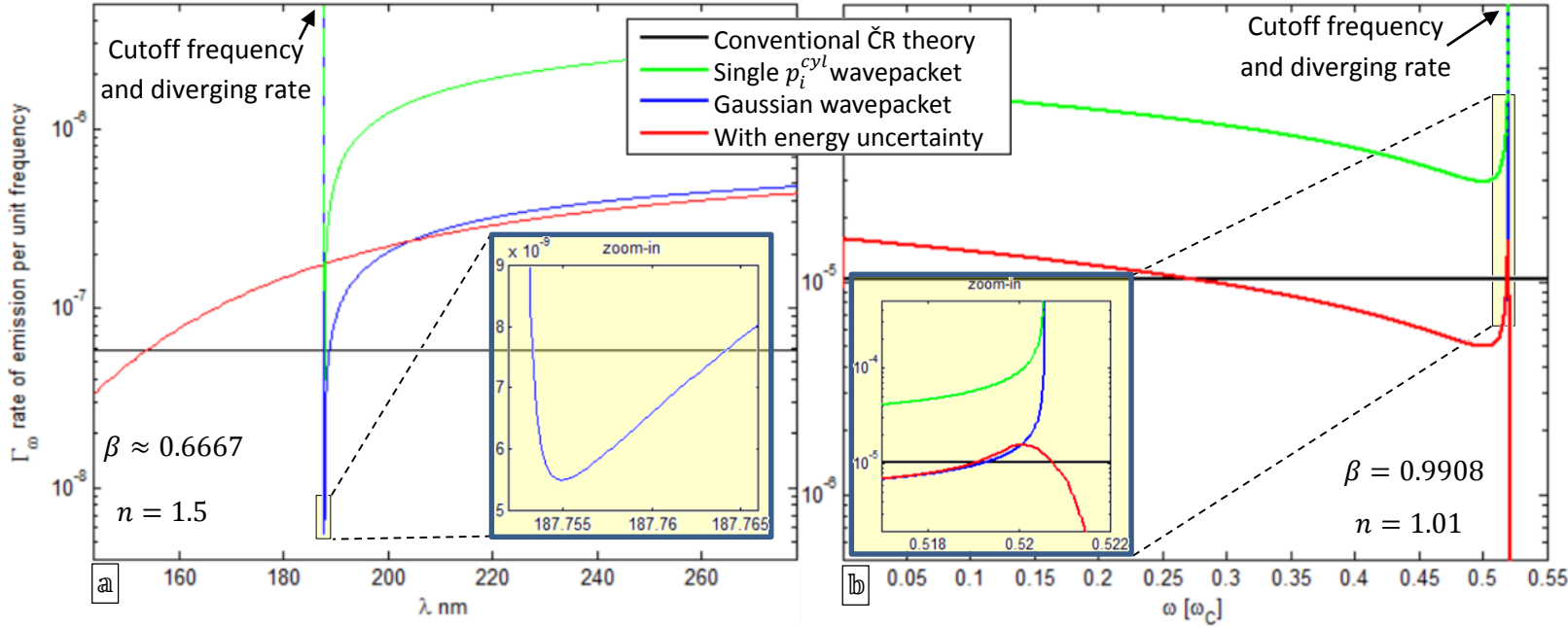
In most experimental scenarios, the incoming electron does not have a well-defined spin, and neither the spin of the outgoing electron nor the polarization of the emitted photons are measured. In such a case, we should sum over all possible incoming and outgoing spin and polarization states. The combined result for the total Γ_ω is Eq.7 with $C = C_{total}$:

$$C_{total} = \frac{1}{2} \alpha \beta \left[\left(1 - \frac{1}{\beta^2 n^2} \right) - \left(1 - \frac{\hbar \omega}{E_i} \frac{n^2 + 1}{4} \right) \frac{n^2 - 1}{\beta^2 n^2} \frac{\hbar \omega}{E_i} \right] = \frac{1}{2} \alpha \beta \sin^2(\theta_{\check{C}R}) + \frac{1}{2} \frac{\alpha}{\beta} \left(\frac{\hbar \omega}{E_i} \right)^2 \frac{n^2 - 1}{2} \quad (8)$$

Interestingly, this result is independent of the electron spread angle θ_i , and thus is exactly equal to previous results that were calculated for a plane-wave incoming electron (single momentum state), e.g., [35] equation 6.36 and [36] equation 4.16. Even so, the emerging radiation in our case still directly depends on θ_i both in its emission angle ($\theta_{ph} = |\theta_i \pm \theta_{\check{C}R}|$) and in the rate of emission Γ_ω (due to Eq.7).

Comparing the quantum Čerenkov Effect to the conventional result

Before proceeding, we check that our QED calculations match the conventional result given by Eq.1b when assuming low photon energies $\hbar\omega \ll E_i$ and an incoming electron with zero spread angle $\theta_i = 0$. First, note that we separated Eq.8 into two terms to distinguish the left term, which is dominant when $\hbar\omega \ll E_i$. Second, the limit of $\theta_i = 0$ is where the type I and type II cones merge (see Eq.7), because $p_{ir} = 0$ and so $p_{fr} = k_r$. In this limit, both options in Eq.7 attain the value 1. Together, we get $\Gamma_\omega = \frac{1}{2} \alpha \beta \sin^2(\theta_{\check{C}R})$ for each cone, and since the two cones merge into one, we recover exactly Eq.1b. Nevertheless, near the frequency cutoff this similarity breaks even for low frequencies, as shown by the green curve in Fig.4a. The curve deviates from the conventional ČR (straight black line) by having a diverging resonance around 188nm and by completely disappearing below this wavelength due to the cutoff of Eq.5. A similar deviation, although even more pronounced, is presented by the green curve in the Fig.4b. There, the frequencies are much higher, the refractive index is much closer to 1, and the incoming electron is much more energetic, causing a prominent quantum correction even far from the critical point.



Deviations between classical and quantum ČR theories: the conventional prediction vs. the QED calculations. We plot the photon emission rate for several cases: The conventional ČR result, according to Frank-Tamm – Eq.1b (straight black line). Incoming electron described by a wavepacket of a single cylindrical momentum state with spread angle of $\theta_i = 0.3$ (green curve). Incoming Gaussian wavepacket with spread angle of 5° (blue curve). Incoming Gaussian wavepacket like before, but with a variance in the electron energy of $\Delta E \approx 0.5eV$ (red curve). The yellow insets are zoomed-in sections of each figure, showing a small dip before the cutoff divergence. The left panel presents the ČR in UV frequency, for index of refraction $n = 1.5$ and velocity around $\beta \approx 2/3$. The right panel presents the ČR for gamma-ray frequencies, for index of refraction $n = 1.01$ and velocity $\beta = 9908$.

A realistic scenario: Gaussian wavepacket

Finally, all calculations above are only carried for an incoming electron in a single cylindrical momentum state p_i^{cyl} . What happens for realistic scenarios, which are always described by some wavepacket? We write the initial electron state as a superposition of the cylindrical momentum states, and repeat the QED calculations. Fortunately, the cylindrical symmetry eliminates all cross-terms, allowing us to directly calculate the total emission rate per unit frequency for the wavepacket ($\Gamma_\omega^{wavepacket}$), by an integral over the rates Γ_ω calculated for each cylindrical momentum state. This property of the cylindrical basis is the motivation for its use in this Letter.

We create a Gaussian-like electron wavepacket by integrating over a range of spread angles around zero – the results appear as the blue curves in Figs.4a. The Gaussian wavepacket shows the same cutoff and divergence near the cutoff frequency, with the only noticeable difference being that the rate is lower, in comparison to the single cylindrical state (in green). The reason for this difference is simply that near the cutoff, Eq.7 shows that larger spread angles give a higher rate Γ_ω . Now since the Gaussian is made of a range of spread angles, all smaller than $\theta_i = 0.3$, it is straightforward to understand that it has a lower total rate.

The red curve in each of the panels in Fig.4 is created by integrating over a range of energies (with a Gaussian envelope), over the Gaussian wavepacket from above. This imposes uncertainty in the energy (or velocity) of the electron, and not only in the spatial spread as is done for the blue curve. Therefore, now the wavepacket is Gaussian both in energy and spread angle, which translates to a Gaussian wavepacket both in space and in time. Figure.4a shows that when the energy spread is wide relative to the resonance feature, the divergence is smoothed out, and the cutoff is observed as a gradual drop in the rate. The energy spread is $\Delta E \approx 0.5eV$, which is on the scale of the entire horizontal axis in this figure. Note that this choice of ΔE is conservative – while most transmission electron microscopes work with ΔE on this scale, modern microscopes that are used for EELS measurements reach variances that are almost 100 times better than this value. Figure.4b shows that for higher photon frequencies, such an energy spread does not completely smoothen the resonance feature, hence there is still a noticeable peak remaining for the red curve. Importantly, the results shown in the blue and red curves in Figs.4 are not specific for Gaussians, and appear for any realistic wavepacket we try. This emphasizes that the new effects we predict in

this Letter are general properties of quantum wavepackets, and as such, should appear in nature without intentional shaping of the wavepacket.

Our vision: beyond the Čerenkov Effect

Before closing we would like to discuss the implications of our findings in a broader perspective. Our fully quantum calculation unraveled major deviations from the conventional ČR – in fact deviations that are not limited to specifically designed quantum wavepackets, but instead, occur for any realistic wavepacket. Mathematically, it is clear that these deviations occur due to the charge carrier being described by a wavepacket. But what is the *physical* reason for these findings? The combination of two inherent facts constitutes the physical reasoning: (1) The electron interaction with the photon field is inherently nonlinear, since the spin-polarization term contains ψ^\dagger and ψ . (2) The Čerenkov Effect is extended in space, occurring over the entire medium of propagation - this means that the interaction length greatly exceeds the wavelength of the emitted photon. When combined together, these two facts contradict the closely-held intuition for light-matter interaction, which is based on the dipole-approximation. The logic of the dipole-approximation holds only when the interacting quantum system is much smaller than the photon wavelength. Here, this only holds as long as the charge carrier is a point-like particle, and completely breaks down when the wave nature of the charge is considered in the ČR phenomenon and the effects associated with it.

Perhaps even more important is the vision this new understanding presents: a realistic particles is never just a single momentum state, therefore, *any scattering process might involve a similar correction that follows from the particle wave structure*. The correction will be significant, and

might even include hidden resonances, given that the process length scale is not exceedingly larger than that of the wavefunctions of the particles involved. This happens in other electron-photon interactions (e.g. Compton effect), but is not limited to these, and can in principle happen in any scattering process in particle physics when there is enough uncertainty in the positions of the particles. The first hints of some quantum wave corrections were actually already noted more than 20 years ago in a series of works by Kotkin, Serbo, and Schiller (e.g. [42,43]). Recently, giving a different point of view on this intriguing phenomenon, are several inspiring papers by Ivanov (e.g. [44,45]) that study how an artificial design of the interacting particle wavepacket as a vortex can greatly enhance specific scattering amplitudes.

Finally, following our predicted divergence in the emission rate, we expect higher-order Feynman diagrams to become important near the frequency cutoff. This points to the possibility of experiments in optics involving only modest electron energies measuring inherent QED effects. This opens-up new regimes of physics that were so far exclusive to the billion-dollar high energy physics experiments.

Acknowledgements

We would like to thank Prof. Robert L. Jaffe and Prof. Levi Schächter for fruitful discussions. We also thank Prof. Francois Ziegler and Prof. Carlo Beenakker for a valuable suggestion regarding the triple-Bessel integral.

Part of the research leading to these results has received funding from the European Union's - Seventh Framework Programme (FP7- Marie Curie IOF) under grant agreement n° 328853 – MC-BSiCS.

References

- [1] Cherenkov, P. A. Visible emission of clean liquids by action of γ radiation. *Dokl. Akad. Nauk SSSR* **2**, 451 (1934).
- [2] Jelley, J. V. Cerenkov radiation and its applications. *Brit. J. Appl. Phys.* **6**, 227 (1955).
- [3] Gordon C. M. & Hoover J. I. Cerenkov radiation fission product detector. *U.S. Patent 2954473*, issued Sep. 27 (1960).
- [4] Séguinot, J. & Ypsilantis, T. Photo-ionization and Cherenkov ring imaging. *Nuclear Instruments and Methods* **142**, 377-391 (1977).
- [5] Ekelöf, T., Seguinot, J., Tocqueville, J., & Ypsilantis, T. The Cerenkov ring-imaging detector: recent progress and future development. *Physica Scripta* **23**, 718 (1981).
- [6] Apsimon, R. J., et al. The recent operational performance of the CERN omega ring imaging Cerenkov detector. *Nuclear Science, IEEE Transactions* **33** 122-131 (1986).
- [7] Casper, D., et al. Measurement of atmospheric neutrino composition with the IMB-3 detector. *Phys. Rev. Lett.* **66**, 2561 (1991).
- [8] Sauli, F. GEM: A new concept for electron amplification in gas detectors. *Nucl. Instrum. Meth. A.* **386**, 531-534 (1997).
- [9] Galbraith, W. & Jelley, J. V. Light pulses from the night sky associated with cosmic rays. *Nature* **171**, 349-350 (1953).
- [10] Vavilov Yu. N., Pugacheva. G. I., Fedorov V. M. m-meson groups near the axis of board atmospheric showers. *Sov. Phys. JETP* **17**, 333 (1963).
- [11] Schächter, L. *Beam-wave interaction in periodic and quasi-periodic structures*. Springer (2011).
- [12] Dohager, R. S., et al. Cerenkov radiation energy transfer (CRET) imaging: a novel method for optical imaging of PET isotopes in biological systems. *PloS one* **5**, e13300 (2010).
- [13] Robertson, R., Germanos, M. S., Li, C., Mitchell, G. S., Cherry, S. R. & Silva, M. D. Optical imaging of Cerenkov light generation from positron-emitting radiotracers. *Physics in medicine and biology* **54**, N355 (2009).
- [14] Luo, C., Ibanescu, M., Johnson, S. G. & Joannopoulos, J. D. Cerenkov radiation in photonic crystals. *Science* **299**, 368-371 (2003).
- [15] Xi, S., Chen, H., Jiang, T., Ran, L., Huangfu, J., Wu, B. I., Kong, J. A. & Chen, M. Experimental verification of reversed Cherenkov radiation in left-handed metamaterial. *Phys. Rev. Lett.* **103**, 194801 (2009).
- [16] Tamm I. E. & Frank I. M., Coherent in-medium fast-electron radiation. *Dokl. Akad. Nauk USSR* **14**, 109-114 (1937).
- [17] Jauch, J. M. & Watson, K. M. Phenomenological quantum electrodynamics. Part II. Interaction of the field with charges. *Phys. Rev.* **74**, 1485 (1948).
- [18] Neamtan, S. M. The Čerenkov Effect and the Dielectric Constant. *Phys. Rev.* **92**, 1362 (1953).
- [19] Tidman, D. A. A quantum theory of refractive index, Čerenkov radiation and the energy loss of a fast charged particle. *Nuclear Physics* **2**, 289-346 (1957).
- [20] Salamon, M. H., Ahlen, S. P. & Tarlé, G. Experimental limits on deviations from Z² dependence of Čerenkov radiation by heavy ions *Phys. Rev. A* **21**, 1506 (1980).
- [21] Schwinger, J., Tsai, W.-Y. & Erber, T. Classical and quantum theory of synergic synchrotron-Čerenkov radiation. *Annals of Physics* **96**, 303-332 (1976).
- [22] Erber, T., White, D., Tsai, W.-Y. & Latal, H. G. Experimental Aspects of Synchrotron-Čerenkov Radiation. *Annals of Physics* **102**, 405-447 (1976).

- [23] Lehnert, R. & Potting, R. Vacuum Čerenkov Radiation. *Phys. Rev. Lett.* **93**, 110402 (2004).
- [24] Altschul, B. Vacuum Čerenkov Radiation in Lorentz-Violating Theories Without CPT Violation. *Phys. Rev. Lett.* **98**, 041603 (2007).
- [25] Jones, F. C. Lorentz-invariant formulation of Cherenkov radiation by tachyons. *Phys. Rev. D* **6**, 2727 (1972).
- [26] Mignani, R. & Recami, E. Tachyons do not emit Čerenkov radiation in vacuum. *Lettere Al Nuovo Cimento (1971–1985)* **7**, 388-390 (1973).
- [27] Bliokh, K. Y., Bliokh, Y. P., Savel'ev, S. & Nori, F. Semiclassical dynamics of electron wave packet states with phase vortices. *Phys. Rev. Lett.*, **99**, 190404 (2007).
- [28] Uchida, M. & Tonomura, A. Generation of electron beams carrying orbital angular momentum. *Nature* **464**, 737–739 (2010).
- [29] Verbeeck, J. Tian, H. & Schattschneider, P. Production and application of electron vortex beams. *Nature* **467**, 301–304 (2010).
- [30] McMorrnan, B. J., et al. Electron vortex beams with high quanta of orbital angular momentum. *Science* **331**, 192–195 (2011).
- [31] Voloch-Bloch, N., Lereah, Y., Lilach, Y., Gover, A. & Arie, A. Generation of electron Airy beams. *Nature* **494**, 331–335 (2013).
- [32] Landau, L. D., Bell, J. S., Kearsley, M. J., Pitaevskii, L. P., Lifshitz, E. M. & Sykes, J. B. *Electrodynamics of continuous media (Vol. 8)*. Elsevier (1984).
- [33] Bliokh, K. Y., Dennis, M. R. & Nori, F. Relativistic Electron Vortex Beams: Angular Momentum and Spin-Orbit Interaction. *Phys. Rev. Lett.* **107**, 174802 (2011).
- [34] Manuscript in preparation
- [35] Harris, E. G. *A pedestrian approach to quantum field theory*, John Willey and Sons, Inc., New York, London (1972).
- [36] Erber, T. & Latal, H. G. Unified radiation formulae for classical and quantum electrodynamics. *European journal of physics* **24**, 67 (2003).
- [37] Gervois, A. & Navelet, H. Some integrals involving three Bessel functions when their arguments satisfy the triangle inequalities. *J. Math. Phys.* **25**, 3350-3356 (1984).
- [38] Ivanov, I. P. Colliding particles carrying nonzero orbital angular momentum. *Phys. Rev. D* **83**, 093001 (2011).
- [39] Ivanov, I. P. & Serbo, V. G. Scattering of twisted particles: Extension to wave packets and orbital helicity. *Phys. Rev. A* **84**, 033804 (2011).
- [40] S. K. H. Auluck, On the Integral of the Product of Three Bessel Functions over an Infinite Domain, *The Mathematica Journal*, 14–15 (2012).
- [41] Cox, R. T. Momentum and Energy of Photon and Electron in the Čerenkov Radiation. *Phys. Rev.* **66**, 106 (1944).
- [42] Kotkin, G. L., Polityko, S. I., Schiller, A. & Serbo, V. G. Influence of the transverse beam sizes on the $ep \rightarrow e\gamma$ cross section at the {HERA} and a Future {CERN} electron-proton collider. *Z. Phys. C* **39**, 61-63 (1988).
- [43] Kotkin, G. L., Serbo, V. G. & Schiller, A. Processes with large impact parameters at colliding beams. *Int. J. Mod. Phys. A* **7**, 4707-4745 (1992).
- [42] Ivanov, I. P. Measuring the phase of the scattering amplitude with vortex beams. *Phys. Rev. D* **85**, 076001 (2012).
- [43] Ivanov, I. P. High-energy physics with particles carrying non-zero orbital angular momentum. *Few-Body Systems* **53**, 167-172 (2012).